Probability density function of steady state concentration in two-dimensional heterogeneous porous media

Olaf A. Cirpka,[1] Felipe P. J. de Barros,[2] Gabriele Chiogna,[3] and Wolfgang Nowak[4]

Received 4 April 2011; revised 27 September 2011; accepted 8 October 2011; published 23 November 2011.

[1] Spatial variability of hydraulic aquifer parameters causes meandering, squeezing, stretching, and enhanced mixing of steady state plumes in concentrated hot-spots of mixing. Because the exact spatial distribution of hydraulic parameters is uncertain, the spatial distribution of enhanced mixing rates is also uncertain. We discuss how relevant the resulting uncertainty of mixing rates is for predicting concentrations. We develop analytical solutions for the full statistical distribution of steady state concentration in two-dimensional, statistically uniform domains with log-hydraulic conductivity following an isotropic exponential model. In particular, we analyze concentration statistics at the fringes of wide plumes, conceptually represented by a solute introduced over half the width of the domain. Our framework explicitly accounts for uncertainty of streamline meandering and uncertainty of effective transverse mixing (defined at the Darcy scale). We make use of existing low-order closed-form expressions that lead to analytical expressions for the statistical distribution of local concentration values. Along the expected position of the plume fringe, the concentration distribution strongly clusters at its extreme values. This behavior extends over travel distances of up to tens of integral scales for the parameters tested in our study. In this regime, the uncertainty of effective transverse mixing is substantial enough to have noticeable effects on the concentration probability density function. At significantly larger travel distances, intermediate concentration values become most likely, and uncertainty of effective transverse mixing becomes negligible. A comparison to numerical Monte Carlo simulations of flow and solute transport show excellent agreement with the theoretically derived expressions.

Citation: Cirpka, O. A., F. P. J. de Barros, G. Chiogna, and W. Nowak (2011), Probability density function of steady state concentration in two-dimensional heterogeneous porous media, *Water Resour. Res., 47*, W11523, doi:10.1029/2011WR010750.

1. Introduction

[2] Aquifers are well known to exhibit structures on multiple scales, leading to spatial variability of hydraulic properties. At practically all sites of interest, the characterization of the subsurface has remained incomplete so that predictions of hydraulic heads, velocities, and solute concentrations remain uncertain. Quantifying spatial variability and uncertainty requires a probabilistic analysis of aquifer properties and dependent state variables. Even though limited in its ability to capture hierarchical structures, two-point geostatistics have been established as standard framework to address questions of stochastic subsurface hydrology [*Dagan*, 1989; *Gelhar*, 1993; *Zhang*, 2002; *Rubin*, 2003].

[3] Solute transport applications have been a particular motivation for stochastic analyses of aquifers. Traditional macrodispersion research analyzed the development of spatial or temporal moments of ensemble-mean solute plumes [e.g., *Gelhar and Axness*, 1983; *Dagan*, 1984; *Neuman et al.*, 1987], which may be used to estimate the expected value of concentration. Conceptually, the expected value of concentration is obtained by averaging over all possible realizations of solute plumes. Unfortunately, at a specific site there is only a single plume, rather than an ensemble. While under favorable conditions the ensemble mean of concentration may be representative for a volume or cross-sectional average, it will hardly be observed at an individual point within an aquifer.

[4] Point-related concentrations, however, are decisive for reaction processes. Therefore, many applications featuring reactive transport require additional probabilistic information about the predictive uncertainty of solute concentrations. In this context, "point-related" concentrations are defined via infinitesimally small volumes on the Darcy scale. Such point-related concentrations are not (yet) the true physical concentrations within individual pores where reactive transport poses the actual requirement of mixing. However, they justify to use the corresponding effective reaction rates for porous media that can be assessed in laboratory tests with homogeneous specimen on the Darcy-scale. A second motivation to look at point statistics is risk assessment. In risk assessment, it might be necessary to approximate the probability that a certain threshold value of concentration is exceeded [e.g.,

[1]Center for Applied Geoscience, University of Tübingen, Tübingen, Germany.
[2]Department of Geotechnical Engineering and Geosciences, Universitat Politecnica de Catalunya-BarcelonaTech, Barcelona, Spain.
[3]Dipartimento di Ingegneria Civile ed Ambientale, University of Trento, Trento, Italy.
[4]Institute of Hydraulic Engineering (LH2)/SimTech, University of Stuttgart, Stuttgart, Germany.

0043-1397/11/2011WR010750

Rubin et al., 1994]. For this purpose, existing ensemble statistics such as the concentration mean and variance are insufficient, because at least an educated guess about the functional shape of the full statistical distribution is needed.

[5] The perturbative framework used in Eulerian methods of macrodispersion has been extended by *Kapoor and Gelhar* [1994a, 1994b] to estimate the local concentration variance in addition to the expected (ensemble mean) value. The validity of the approach, however, has been questioned because the relationship between the random velocity and concentration fields is highly nonlinear, and difficult-to-justify closures were needed for approximating expected values of random triple products. Following the Lagrangian framework, the concentration variance was evaluated from spatial moments of one- and two-particle displacements in conjunction with assumptions about the functional shape of the displacement distributions (*Pannone and Kitanidis* [1999], *Fiori and Dagan* [2000], *Vanderborght* [2001], and *Tonina and Bellin* [2008], among others).

[6] The range of possible concentration values is always bounded at 0, and often exhibits an upper bound (e.g., by the initial or source-zone concentration of an injected plume). Mixing of solutes leads to the occurrence of intermediate concentrations. Due to incomplete mixing, a common observation in Monte Carlo simulations of conservative solute plumes is that the most likely concentration values are close to the extremes (close to 0 and the maximum of the possible range), at least at short travel distances. Such a distribution may be parameterized by a scaled beta distribution [e.g., *Fiorotto and Caroni*, 2002, 2003; *Caroni and Fiorotto*, 2005; *Schwede et al.*, 2008; *Bellin et al.*, 2011]. Similar findings have been published for the turbulent transport of scalars by *Girimaji* [1991]. The choice of the beta distribution for the probability density function (pdf) of concentration in heterogeneous porous media has recently been supported with theoretical evidence based on an Ito Stochastic Differential Equation for local concentration dynamics [e.g., *Bellin and Tonina*, 2007; *Sanchez-Vila et al.*, 2009].

[7] Statistical characterization of concentration has been studied in a variety of fields such as turbulence, combustion and atmospheric sciences [e.g., *Chatwin and Sullivan*, 1990; *Pope*, 1994]. *Pope* [1985] gives a review of pdf-methods developed in these fields of application, including models that rely on a particular functional shape of the pdf, such as the beta distribution, and approaches of formulating governing equations of probability density. The latter type of approaches has been applied to reactive transport in porous media where the uncertainty originated from the reactive parameters and potentially from uncertainty in advective transport [*Lichtner and Tartakovsky*, 2003; *Tartakovsky et al.*, 2009; *Tartakovsky and Broyda*, 2011]. *Meyer et al.* [2010] developed a joint pdf transport equation for conservative transport both in a Lagrangian and an Eulerian framework.

[8] One of the most promising approaches of analytically estimating the concentration pdf in hydraulically heterogeneous porous media makes use of spatial concentration moments, which may be derived from rigorous first-order theory [*Fiori and Dagan*, 2000; *Dentz et al.*, 2000] or inferred by other methods. Even though the Lagrangian and Eulerian approaches differ in their derivation [*Pannone and Kitanidis*, 1999; *Fiorotto and Caroni*, 2002, 2003; *Caroni and Fiorotto*, 2005; *Schwede et al.*, 2008; *Dentz and Tartakovsky*, 2010], the general approach via spatial moments may be interpreted the easiest in the framework of generating solute plumes. From ensemble dispersion (or one-particle moments) and effective dispersion (or two-particle moments), it is possible to approximate the uncertainty of the plume center and the expected spread of an individual plume. Assuming that the spatial concentration distributions of individual plumes have an approximately Gaussian shape in cross sections, and that the statistical distribution of the plume center location is also Gaussian, the probability density function of concentration can be computed by the spatial Gaussian concentration distribution of individual plumes with given center of gravity and the probability density of all possible locations of the plume center.

[9] A particular difficulty in the aforementioned approach is that it neglects the uncertainty of effective dispersion (or that of two-particle moments), controlling the spread of individual plumes. This implies that the individual plumes all show the same degree of dilution. This is in contrast both to observations in highly resolved numerical simulations and to experimental studies showing that solute mixing exhibits strong spatial variability [e.g., *Cirpka and Kitanidis*, 2000; *Rahman et al.*, 2005; *Werth et al.*, 2006; *Rolle et al.*, 2009; *Chiogna et al.*, 2011; *Nowak and Cirpka*, 2006]. In particular, zones with exceptionally high velocity act as hot spots of transverse mixing, because the transverse diffusion length is significantly reduced within such zones. Thus, mixing mainly takes place at only a few locations with uncertain spatial frequency and position. The effect of this uncertainty on the concentration pdf has not yet been studied. It may be worth noting that the uncertainty of actual solute mixing in porous media has only recently been tackled by stochastic-analytical approaches [*de Barros and Rubin*, 2011; *Cirpka et al.*, 2011].

[10] *Cirpka et al.* [2011] derived a stochastic framework of transverse solute mixing at the Darcy scale in two-dimensional heterogeneous domains by switching to streamline coordinates. This approach has a long tradition in river mixing [e.g., *Yotsukura and Sayre*, 1976]. In this framework, transverse mixing may be seen as the probability of a solute particle to jump onto neighboring streamlines while being advected from high to low values of hydraulic head. In their study, *Cirpka et al.* [2011] showed that the expected value of effective transverse dispersion rates is independent of travel distance. They also quantified the uncertainty of transverse mixing, including its spatial trends and correlation.

[11] In the present study, we will consider the full statistical distribution of concentration in a two-dimensional domain under steady state flow and transport conditions. Similar to *Cirpka et al.* [2011], we are also focusing on the Darcy scale. For the ease of the analysis, we limit ourselves to steady state transport (see below). We also restrict ourselves to a uniform-in-the-mean, second-order stationary velocity field in a semi-infinite domain. In order to make use of low-order stochastic-analytical expressions, we assume that the underlying log-hydraulic conductivity field is mildly heterogeneous and has an isotropic, exponential covariance function. In particular, we analyze the situation in which a solute plume is introduced over half the inflow width of a domain. We do this to gain insight into the decisive mixing processes along a single plume fringe, even though we know that most plumes have several fringes that interfere with each other at sufficiently large travel distances.

[12] In such a general setup, an observation point might be located within the plume, where the concentration is maximal, or far outside the plume, where the concentration is close to 0, or at the plume fringe, where intermediate concentrations can be observed. This implies that the concentration statistics depend on the uncertainties of both plume meandering and transverse mixing. The key question to be addressed is the relative importance of these two uncertainties on the concentration pdf.

[13] Like in the approaches mentioned above, we will consider a Gaussian-related shape of individual plumes in the transverse direction. However, we assume this shape to hold in streamline-coordinates rather than in spatial coordinates, which is in accordance to the experimental observations of *Rahman et al.* [2005], and has been applied in river mixing for quite a while [e.g., *Yotsukura and Sayre*, 1976]. We explicitly consider the variability of effective transverse dispersion, assuming a lognormal distribution for the effective rate of transverse mixing. Under these circumstances, we can use the analytical results of *Cirpka et al.* [2011] for the expected value and variance of transverse mixing. To account for the effects of plume meandering on the concentration statistics, we make use of stochastic-analytical results of the stream function mean and covariance function derived by *de Barros and Nowak* [2010], assuming a multi-Gaussian distribution of stream function differences. We derive first-order fully analytical results for the case of deterministic transverse mixing, and semianalytical results for the case including the uncertainty of transverse mixing. Finally, we compare the theoretical concentration pdfs to results of extensive Monte Carlo simulations.

[14] In the present study, we will restrict the analysis to steady state transport. This is motivated by two factors. First, it allows to derive analytical solutions and characteristic length scales of different statistical regimes that offer valuable insights also for more complex systems. Second, contaminant plumes with continuous injection caused, e.g., by nonaqueous phase liquid source zones can often be considered to be close to a steady state. Various studies have attempted to derive analytical expressions for transverse mixing of such (quasi) steady state plumes, how transverse dispersion affects overall reaction rates, and the length to which steady state plumes can grow [*Ham et al.*, 2004; *Liedl et al.*, 2005; *Cirpka et al.*, 2006; *Cirpka and Valocchi*, 2007, 2009; *Cirpka*, 2010, among others]. Most of these analyses were done in two spatial dimensions, considering a vertical cross section in the flow direction of a wide plume.

[15] There is a long list of field studies that analyze plumes at steady state and support this assumption with arguments [e.g., *King and Barker*, 1999; *Thornton et al.*, 2001; *Peter et al.*, 2004; *Maier and Grathwohl*, 2006; *Prommer et al.*, 2006; *Lonborg et al.*, 2006; *Anneser et al.*, 2008]. *King and Barker* [1999] intensively discuss that transient slug-type plumes, as studied in tracer tests, do not adequately reflect typical contaminant plumes. They argue that the slug injection plume will not display aspects of long-term behavior, such as an approach to steady state, which may be of particular interest for plumes originating from fixed sources. *Maier and Grathwohl* [2006] argue that steady state transport can be safely assumed in many sites where either the plume is very old and well developed [e.g., *Lonborg et al.*, 2006], or where the time scale of interest for transport is smaller than the time-scale for significant water table changes [e.g., *Prommer et al.*, 2006]. The assumption of a steady source has been applied even in cases where the plume itself did not reach yet the steady state [e.g., *Thornton et al.*, 2001].

[16] The present contribution does not cover mixing-controlled reactions themselves. However, it is possible to derive improved statistical concentration distributions of mixing-controlled reactive species under specific conditions of the reactive systems, when using our concentration pdfs as input to adequate statistical studies of reactive transport [e.g., *Cirpka et al.*, 2008; *Sanchez-Vila et al.*, 2009; *Bellin et al.*, 2011].

2. Theory

2.1. General Setup

[17] We consider steady state two-dimensional groundwater flow in an infinite domain with uniform aquifer thickness and spatially variable, random and locally isotropic hydraulic conductivity K [L/T]. Let $\mathbf{x} = (x, y)$ [L] denote the Cartesian coordinate system. At each point within the domain, the specific-discharge vector $\mathbf{q}$ [L/T] is defined by Darcy's law:

$$\mathbf{q} = -K\nabla\varphi, \tag{1}$$

in which φ [L] is the hydraulic head. Continuity of fluxes results in the groundwater flow equation:

$$\nabla \cdot (K\nabla\varphi) = 0, \tag{2}$$

subject to the mean hydraulic gradient $\mathbf{J}$:

$$\langle\nabla\varphi\rangle \equiv \mathbf{J} = \begin{bmatrix} J \\ 0 \end{bmatrix}. \tag{3}$$

Here, J [-] is the absolute value of the mean hydraulic gradient oriented into the longitudinal (x) direction, and angle brackets denote the ensemble expectation. The above considerations resemble divergence-free and macroscopically uniform flow fields. The flow field can also be characterized by the stream function ψ, meeting [*Bear*, 1972]:

$$\nabla \cdot \left(\frac{1}{K}\nabla\psi\right) = 0, \quad \text{subject to} \quad \langle\nabla\psi\rangle = \begin{bmatrix} 0 \\ \langle q\rangle \end{bmatrix}. \tag{4}$$

[18] Within this spatially variable (but macroscopically uniform) flow field, we consider a steady state transport scenario:

$$\mathbf{q} \cdot \nabla c - \nabla \cdot (\theta\mathbf{D}\nabla c) = 0, \tag{5}$$

subject to a step-like boundary condition at $x = 0$:

$$c(x = 0, y) = \begin{cases} c_{\text{in}} & \text{if } y < 0 \\ 0 & \text{otherwise} \end{cases}. \tag{6}$$

All other boundaries are considered to be infinitely far away. In equations (5) and (6), c [M/L^3] denotes concentration, c_{in} [M/L^3] is the nonzero concentration at the inlet, θ [-] represents effective porosity, and $\mathbf{D}$ [L^2/T] is the dispersion tensor with principal components D_l (along the mean flow direction) and D_t (transverse to mean flow direction). In the following, all concentrations are normalized by c_{in}, such that

all concentration values range between 0 and 1. The boundary conditions for transport resemble an individual fringe of a plume and are an adequate representation for entire plumes that are wide enough that different fringes do not interact.

[19] The advection-dispersion equation, equation (5), may be rewritten in streamline coordinates [see *Cirpka et al.*, 2011]:

$$-\frac{q^2}{K}\frac{\partial c}{\partial \varphi}-\frac{q}{K}\frac{\partial}{\partial \varphi}\left(\theta D_\ell \frac{q}{K}\frac{\partial c}{\partial \varphi}\right)-q\frac{\partial}{\partial \psi}\left(\theta D_t q\frac{\partial c}{\partial \psi}\right)=0$$

with corresponding step-like boundary condition. Without loss of generality, we choose the streamline coordinates φ and ψ such that they are both 0 at $x = y = 0$.

[20] Figure 1 shows the concentration distribution in a heterogeneous flow field meeting the conditions described above. The solid lines describe streamlines. The heterogeneity of the flow field leads to a distortion of the steady state concentration field, including meandering of the centerline. Previous studies have shown that transverse concentration profiles are difficult to interpret without knowledge of the exact velocity field [*Rahman et al.*, 2005; *Rolle et al.*, 2009; *Chiogna et al.*, 2011]; however, if the transverse coordinate y is replaced by the stream function value ψ, the concentration profile in the given setup resembles quite closely the analytical Fickian profile for a step-like boundary condition [e.g., *Rahman et al.*, 2005]:

$$c(\psi)=\frac{1}{2}\mathrm{erfc}\left(\frac{\psi}{w_\psi\sqrt{2}}\right), \tag{7}$$

in which w_ψ [L^2/T] is the characteristic width of the plume fringe measured in the streamline coordinate, i.e., expressed as cumulative discharge. The validity of equation (7) in heterogeneous flow fields is tested in Appendix C. In case of a homogeneous flow field, w_ψ^2 is determined by [see *Cirpka et al.*, 2011]:

$$w_\psi^2(x)=2\theta JKD_t x. \tag{8}$$

[21] The effect of heterogeneity is twofold. First, it leads to the distortion of the concentration profile according to streamline meandering. This effect can be addressed by considering the statistics of stream function values when mapping the assumed cross-sectional error functions back from streamline coordinates to Cartesian coordinates. Second, the spatial variability of the stream function field causes variability of effective transverse mixing, which we express as the probability

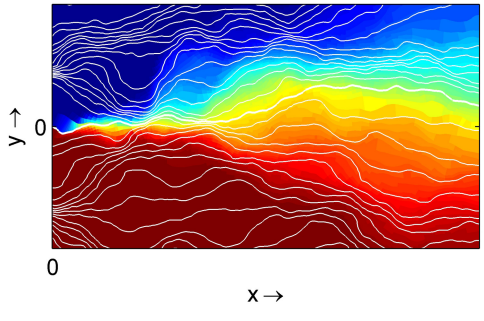

Figure 1. Steady state concentration distribution in an individual realization. Color coding: normalized concentration; solid lines: streamlines; bold line: bounding streamline of the plume.

that a solute particle jumps from a specific streamline to a neighboring one. *Werth et al.* [2006] have illustrated that the net effect of heterogeneity is a slight enhancement of transverse mixing. *Cirpka et al.* [2011] developed analytical expressions of the space-dependent expected value and uncertainty of mixing in two-dimensional heterogeneous flow fields with uniform mean velocity, represented by the mean and variance of the squared fringe width w_ψ^2.

2.2. Statistics of Stream Function Value ψ and Squared Width w_ψ^2 of the Fringe

[22] For analyzing the stream function values ψ at locations $\mathbf{x} = (x, y)$ we choose the system such that $\psi = 0$ lies at the origin of the system of coordinates. Then, for a mean hydraulic gradient oriented into the x-direction, the expected value μ_ψ [L^2/T] of ψ is

$$\mu_\psi(x,y)=K_g J y. \tag{9}$$

[23] The variance σ_ψ^2 [L^4/T^2] of ψ can be approximated using the functional similarity of potential and stream function fields. The variance of the stream function–difference at (x, y) with respect to the origin is twice the semivariogram value of ψ for the given distance vector, which is very closely related to the semivariogram function γ_ψ [L^2] of the potential field [see *de Barros and Nowak*, 2010]:

$$\sigma_\psi^2(x,y)=2K_g^2\gamma_\varphi(y,x). \tag{10}$$

[24] Closed-form, low-order expressions of γ_ψ for specific covariance models of log-hydraulic conductivity have been derived [e.g., *Dagan*, 1985; *Rubin*, 2003, pp. 97–98]. Please note that we have exchanged the coordinate arguments of γ_ψ from (x, y) to (y, x) in order to obtain a stream function variance. This exchange reflects a rotation of the head variogram by 90°. Appendix A includes the corresponding first-order expression of σ_ψ^2 for an isotropic, exponential covariance model of log conductivity.

[25] Numerical experiments, shown in Appendix C, indicate that the statistical distribution of ψ at a sufficient distance may well be approximated by a Gaussian distribution with mean μ_ψ and variance σ_ψ^2:

$$p(\psi)=\frac{1}{\sigma_\psi\sqrt{2\pi}}\exp\left[-\frac{(\psi-\mu_\psi)^2}{2\sigma_\psi^2}\right]. \tag{11}$$

The above statement can also be supported by transverse particle displacement statistics in Lagrangian studies [*Dagan*, 1987; *Fiori and Dagan*, 2000]. The assumption of multi-Gaussianity is reasonable for low to mildly heterogeneous aquifers only.

[26] The statistics of the squared fringe width w_ψ^2 in stream function values have been analyzed by *Cirpka et al.* [2011] using low-order perturbative methods. The key results regarding the mean $\mu_{w_\psi^2}$ and variance $\sigma^2_{w_\psi^2}$ read as

$$\mu_{w_\psi^2}(x)\approx 2\theta Jx\langle KD_t\rangle, \tag{12}$$

$$\sigma^2_{w_\psi^2}(x)\approx 4J^2\theta^2\int_0^x\int_0^x\langle\mathcal{B}(x^*)\mathcal{B}(x^{**})\rangle dx^*dx^{**}, \tag{13}$$

with

$$\mathcal{B}(x^*)=[K(x^*)D_t(x^*)-\langle K(x^*)D_t(x^*)\rangle]. \tag{14}$$

Closed-form expressions for the case of local transverse dispersion (with Scheidegger-type linear dependence on the velocity) are reported in Appendix B. Based on numerical evidence, shown in Appendix C, $p\left(w_\psi^2\right)$ may be approximated by a lognormal distribution if K is lognormal:

$$p(w_\psi^2) = \frac{1}{w_\psi^2 \sigma_{\ln w_\psi^2}\sqrt{2\pi}} \exp\left(-\frac{\left(\ln w_\psi^2 - \mu_{\ln w_\psi^2}\right)^2}{2\sigma_{\ln w_\psi^2}^2}\right), \tag{15}$$

in which $\mu_{\ln w_\psi^2}$ and $\sigma_{\ln w_\psi^2}^2$ are the mean and variance of $\ln\left(w_\psi^2\right)$. They can be computed from the mean $\mu_{w_\psi^2}$ [L^4/T^2] of w_ψ^2 and its coefficient of variation $CV_{w_\psi^2}$ [-] via the well-known relations between the moments of Gaussian and corresponding lognormal variables:

$$\sigma_{\ln w_\psi^2}^2 = \ln\left(1 + CV_{w_\psi^2}^2\right) \tag{16}$$

$$\mu_{\ln w_\psi^2} = \ln\left(\mu_{w_\psi^2}\right) - \frac{1}{2}\sigma_{\ln w_\psi^2}^2. \tag{17}$$

2.3. Concentration PDF

[27] According to equation (7), at any given location $\mathbf{x} = (x, y)$, the uncertainty of concentration c is caused by that of the stream function value ψ and that of the degree of mixing, w_ψ^2. As a first step, in analogy to *Dentz and Tartakovsky* [2010], we start with the uncertainty in concentration that is caused only by the uncertainty in plume position, that is, the uncertainty of ψ. The novelty we provide in our first step is to map an analytical assumption for concentration values in cross sections of the plume (equation (7)) to the stream function coordinate, instead of mapping it to the y coordinate.

[28] Because the functional dependence $c(\psi)$ in equation (7) is monotonic for any given value of w_ψ^2, the conditional statistical distribution $p\left[c(\psi)|w_\psi^2\right]$ can be obtained by standard rules of pdf mapping:

$$p\left[c(\psi)|w_\psi^2\right] = \left|\frac{\partial\psi}{\partial c(\psi)}\right| p(\psi). \tag{18}$$

[29] Substituting equations (7) and (11) into equation (18) and rearranging terms yields:

$$p(c|w_\psi^2) = \frac{w_\psi}{\sigma_\psi} \exp\left\{\left[\mathrm{erfc}^{-1}(2c)\right]^2 - \left[\mathrm{erfc}^{-1}(2c) - \frac{\mu_\psi}{w_\psi\sqrt{2}}\right]^2 \frac{w_\psi^2}{\sigma_\psi^2}\right\}, \tag{19}$$

in which $\mathrm{erfc}^{-1}(2c)$ is the inverse complimentary error function of $2c$, w_ψ^2, and σ_ψ^2 depend on x, and μ_ψ depends on y. Later, we will insert equation (9) for μ_ψ, equation (10) for σ_ψ^2, and express w_ψ^2 either by its mean value according to equation (12) or integrate over the distribution $p(w_\psi^2)$ according to equation (15).

[30] Equation (19) exhibits two regimes, which may best be addressed for the case of $\mu_\psi = 0$, referring to a point on the centerline of the ensemble averaged plume fringe. Then, if the uncertainty in the stream function value is higher than the spread of individual plumes, i.e., $\sigma_\psi > w_\psi$, the probability density is the highest at the two limiting concentrations, $c = 0$ and $c = 1$. This is most likely the case at locations close to the inlet boundary. Here, plume meandering lets a point mainly sample the extreme values of concentration. By contrast, if the plumes in individual realizations are sufficiently diluted, i.e., $\sigma_\psi > w_\psi$, the probability density is the highest at the center value $c = 0.5$. In the special case of $\mu_\psi = 0$ and $\sigma_\psi = w_\psi$, the resulting distribution $p(c|w_\psi^2)$ is uniform. These observations are illustrated in Figure 2 (top).

[31] Figure 2 (bottom) refers to a point with a systematic offset in the lateral coordinate toward smaller c-values, $\mu_\psi/w_\psi = 1$. Here, cases with high relative uncertainty of ψ (i.e., $\sigma_\psi > w_\psi$) also lead to maximum probability densities at the extreme values, but the distribution is not symmetric. In the transition between the regimes of $\sigma_\psi > w_\psi$ and $\sigma_\psi < w_\psi$, i.e., for the special case of $\sigma_\psi = w_\psi$, the lower physical limit $c = 0$ is still the most likely value, whereas the upper limit of $c = 1$ has a probability density of 0. Finally, in the case of smooth individual plumes, $\sigma_\psi < w_\psi$, the conditional concentration distribution $p(c|w_\psi^2)$ becomes unimodal with the peak at some intermediate concentration value.

[32] As our second step, we obtain a more accurate pdf of concentration that also considers the uncertainty in mixing. To this end, we marginalize $p(c|w_\psi^2)$ over $p(w_\psi^2)$:

$$p(c) = \int_0^\infty p(c|w_\psi^2)p(w_\psi^2)dw_\psi^2, \tag{20}$$

which results, for the assumed lognormal distribution of $p(w_\psi^2)$ for the squared fringe width, in the following expression:

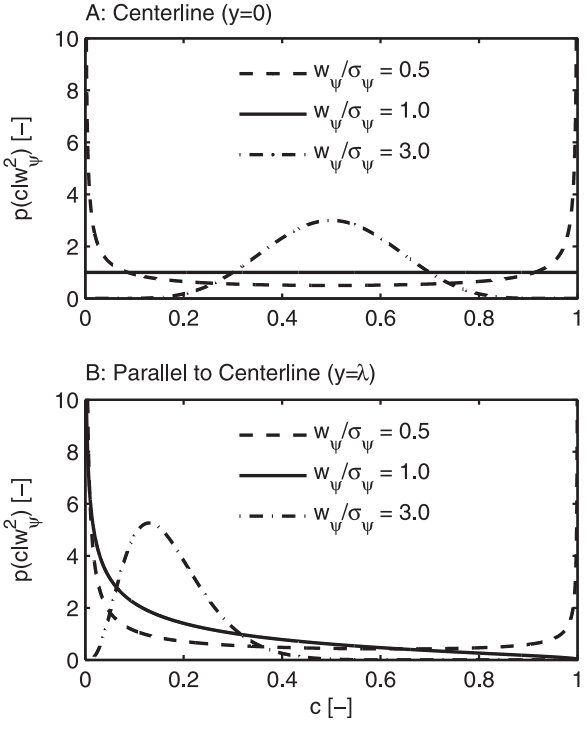

Figure 2. Concentration pdf $p(c|w_\psi^2)$ for various given ratios w_ψ/σ_ψ. (top) $\mu_\psi/w_\psi = 0$ (centerline); (bottom) $\mu_\psi/w_\psi = 1$ (offset toward smaller c-values).

$$p(c) = \frac{1}{\sigma_\psi \sigma_{\ln w_\psi^2}\sqrt{2\pi}} \times \int_0^\infty \frac{1}{w_\psi} \exp\left\{ \left[\mathrm{erfc}^{-1}(2c)\right]^2 - \left[\mathrm{erfc}^{-1}(2c) - \frac{\mu_\psi}{w_\psi\sqrt{2}}\right]^2 \frac{w_\psi^2}{\sigma_\psi^2} - \frac{\left(\ln w_\psi^2 - \mu_{\ln w_\psi^2}\right)^2}{2\sigma_{\ln w_\psi^2}^2} \right\} dw_\psi^2. \quad (21)$$

[33] The above expression is our final analytical result for the concentration pdf. In the following application, we perform the remaining integration of equation (21) numerically by evaluating the 1000 values of w_ψ^2 with cumulative probability of [0.5, 1.5, ... 999.5]/1000 according to the underlying lognormal distribution, computing the conditional pdf of concentration $p(c|w_\psi^2)$ for each value of w_ψ^2, and finally averaging over the set of w_ψ^2-values.

[34] Figure 3 shows an example calculation for the marginalized pdf of concentration $p(c)$ according to equation (21). The location is slightly off the centerline of the mean plume fringe. Here, equation (19) predicted a unimodal pdf of $p(c|w_\psi^2)$ when neglecting the uncertainty of mixing, as shown by the dashed line. The solid line refers to our concentration pdf $p(c)$ with uncertainty in mixing according to equation (21). For a simple first illustration, we consider a coefficient of variation in w_ψ^2 of $CV_{w_\psi^2} = 0.75$. The uncertainty in w_ψ^2 has two effects. First, the extreme values ($c = 0$ and $c = 1$) are the most likely values for all cases in which $w_\psi^2 < \sigma_\psi^2$. Even though the expected value of w_ψ^2 is 1.5 times σ_ψ^2 in our example, the probability of $w_\psi^2 < \sigma_\psi^2$ is significant. This results in a marginalized distribution $p(c)$ with maximum probability density at the extremes. Second, there is also a substantial probability that w_ψ^2 is much larger than $\mu_{w_\psi^2}$. In these cases, $p(c|w_\psi^2)$ is more peaked than $p(c|w_\psi^2 = \mu_{w_\psi^2})$. The net effect on the marginalized distribution $p(c)$ is a shoulder at intermediate values of c.

3. Application and Discussion

3.1. Analytical Results

[35] We now apply the analytical approach to a hypothetical test case of an infinite two-dimensional aquifer with second-order stationary log conductivity field and uniform mean hydraulic gradients. Dimensionless parameters characterizing the test case are listed in Table 1. Figure 4 shows length profiles of key statistical parameters determining the pdf of concentration, namely (1) the variance σ_ψ^2 of the stream function value along the centerline of the mean plume fringe according to equation (A5), shown as solid line, (2) the expected value $\mu_{w_\psi^2}$ of the squared width w_ψ^2 of the plume fringe according to equation (B2), shown as dashed line; and (3) the standard deviation $\sigma_{w_\psi^2}$ of w_ψ^2 according to equations (B2) and (B3), shown as dash-dotted line. The length coordinate is scaled by the correlation length λ [L], and the dependent variables are all normalized by $(K_g J \lambda)^2$.

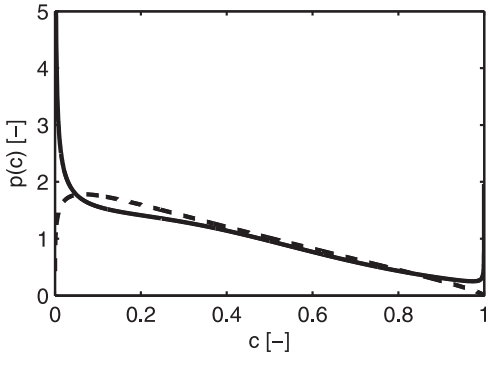

Figure 3. Marginalized pdf of concentration $p(c)$ considering a lognormal distribution of the squared fringe width w_ψ^2. Parameters: $\mu_\psi^2/\mu_{w_\psi^2} = 0.25$, $\mu_{w_\psi^2}/\sigma_\psi^2 = 1.5$; solid line: $CV_{w_\psi^2} = 0.75$; dashed line: $CV_{w_\psi^2} = 0$ (no uncertainty of w_ψ^2).

Table 1. Dimensionless Numbers Characterizing the Example Application AQ1

Parameters	Value
Physical Parameters	
Péclet number for pore diffusion	$Pe_p = \frac{JK_g\lambda}{D_p\theta} = 2000$
Péclet number for transverse hydromechanical dispersion	$Pe_{t,mech} = \frac{\lambda}{\alpha_t} = 100$
Variance of log-conductivity	$\sigma_Y^2 = 1$
Numerical Discretization	
Dimension of the domain	$\frac{L_x}{\lambda} \times \frac{L_y}{\lambda} = 300 \times 40$
Grid spacing	$\frac{\Delta x}{\lambda} = \frac{\Delta y}{\lambda} = 0.1$

[36] First, we analyze characteristic regimes of concentration statistics without uncertainty in mixing, i.e., fixing the squared width of the plume fringe in equation (21) to its expected value, $w_\psi^2(x) = \mu_{w_\psi^2}(x)$. Formally, this results in a conditional concentration pdf $p(c|w_\psi^2 = \mu_{w_\psi^2})$.

[37] At small distances, the uncertainty of plume meandering, indicated by σ_ψ^2, increases rapidly, while the expected squared fringe width $\mu_{w_\psi^2}$ increases more slowly. As we have discussed above, this regime leads to a conditional probability density function $p(c|w_\psi^2 = \mu_{w_\psi^2})$ of concentration with highest probability density at the extremes. The leading term within σ_ψ^2 is $\ln(x/\lambda)$, whereas $\mu_{w_\psi^2}$ increases linearly. Considering the model parameters specific of this study, at about 56 correlation lengths, the expected width of the plume fringe reaches the level of the uncertainty in

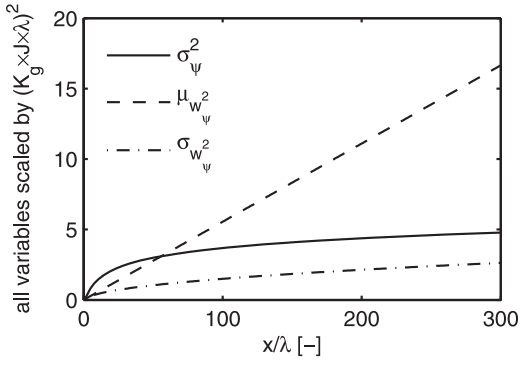

Figure 4. Statistical measures determining the concentration pdf along the centerline of the mean plume fringe. Solid line, σ_ψ^2: variance of stream function value ψ; dashed line, $\mu_{w_\psi^2}$: expected value of the squared fringe width in stream function values; dash-dotted line, $\sigma_{w_\psi^2}$: standard deviation of the squared fringe width in stream function values.

plume meandering, i.e., $\mu_{w^2_\psi} = \sigma^2_\psi$. At larger distances, equation (19) states that the conditional probability density function $p(c|w^2_\psi = \mu_{w^2_\psi})$ of concentration along the centerline $y = 0$ must be unimodal with the mode being 0.5. Figure 4 also shows the uncertainty $\sigma_{w^2_\psi}$ of w^2_ψ, which has a leading term of $\sqrt{x/\lambda}$. At some point in very large distance not shown in Figure 4, the uncertainty of mixing $\sigma_{w^2_\psi}$ becomes larger than the uncertainty of plume meandering σ^2_ψ. This point is within the regime where plume meandering is small in comparison to the width of the plume fringe, i.e., beyond 56 correlation lengths for our set of parameters.

[38] Now, we analyze the impact of uncertainty in mixing on the resulting shape of our analytical concentration pdf. We will compare our analytical expression to numerical results in section 3.2. Figure 5 shows different concentration pdfs (equations (19) and (21), numerical) as function of distance along the centerline of the mean plume fringe (Figures 5a, 5c, 5e) and at a distance of one correlation length parallel to it (Figures 5b, 5d, 5f). Figures 5a and 5b show the analytical conditional distribution $p(c|w^2_\psi = \mu_{w^2_\psi})$ according to equation (19), neglecting the uncertainty of the mixing and fringe width. Figures 5c and 5d show the analytical marginalized distribution $p(c)$ according to equation (21), i.e., with uncertainty of mixing and fringe width. Figures 5e and 5f refer to numerical results for later comparison (see section 3.2). The general shapes of the analytical pdfs reflect the regimes discussed above.

[39] The profiles along the centerline (Figures 5a, 5c, and 5e) are symmetric about the expected value of $c = 0.5$, whereas the profiles parallel to the centerline (Figures 5b, 5d, and 5f) are asymmetric and exhibit an expected value of c depending on distance. In our case, at distances $x \lessapprox 56\lambda$, the extreme concentration values are the most likely ones, whereas for larger distances intermediate concentration values become more likely. For the marginalized distribution $p(c)$, shown in Figures 5c and 5d, the regime with high probability density at the extreme values prevails over a larger distance, while the conditional distributions $p(c|w^2_\psi = \mu_{w^2_\psi})$ in Figures 5a and 5b leave this regime already at shorter travel distances. A sharp transition between the two regimes is visible at $\mu_{w^2_\psi} = \sigma^2_\psi$ as a straight white isoline in Figure 5a. It should be noted that we have limited the maximum value of probability density plotted in Figure 5 to 5 in order to better visualize the general trend. We have computed and observed much higher values close to the extreme values of the concentration range for short travel distances.

[40] In principle, the analytical distributions neglecting and accounting for the uncertainty of w^2_ψ look very similar. To obtain an objective measure of agreement between the two distributions, we computed the mean absolute error (MAE) MAE(p) introduced by neglecting the uncertainty of w^2_ψ:

$$\mathrm{MAE}(p) = \int_0^1 \left| p(c) - p(c|w^2_\psi = \mu_{w^2_\psi}) \right| dc, \qquad (22)$$

which is plotted as function of distance in Figure 6. The argument of the integral in equation (22) may be infinite at the limits $c = 0$ and $c = 1$ for short travel distances, but the integral is finite. We have also tested the mean square error as metric, but the latter is too dominated by the behavior close to the extreme values. Considering that the mean $p(c)$ value of both distributions is unity, Figure 6 shows that the error introduced by using the conditional concentration distribution, $p(c|w^2_\psi = \mu_{w^2_\psi})$, rather than the marginalized one, $p(c)$, is highly relevant at smaller travel distances. Here, $p(c)$ exhibits an even higher probability of the extreme values than $p(c|w^2_\psi = \mu_{w^2_\psi})$. At larger travel distances, the error introduced by neglecting the uncertainty of w^2_ψ (i.e., of mixing with ambient water) becomes negligible, because the uncertainty due to meandering dominates (compare Figure 4).

3.2. Comparison to Numerical Simulations

[41] In order to test our analytical expressions, we perform Monte Carlo simulations of flow and transport with 10,000 realizations using the same parameters as applied in the analytical methods, listed in Table 1. We generate two-dimensional, random, auto-correlated log conductivity fields by the method of *Dietrich and Newsam* [1993]. On each K-field, the fields of potential φ and stream function ψ are computed by the standard Finite Element Method using bilinear elements [*Frind and Matanga*, 1985]. Fixed-head boundary conditions are applied at the left- and right-hand side boundaries, whereas no-flow conditions are applied at the top and bottom boundaries. Streamline-oriented grids are generated following the approaches of *Frind and Matanga* [1985] and *Cirpka et al.* [1999a]. Steady state solute transport on the streamline-oriented grids is solved by the Finite Volume Method [*Cirpka et al.*, 1999b]. Rather than directly applying the fixed-concentration boundary condition at the inflow boundary of the computational domain, we fix the concentration along a vertical line at 10 integral scales into the domain.

[42] At the bottom half along this profile, the concentration is 1, and at the top half it is 0. In the following analysis, concentrations before the source line (less than ten integral scales away from the upstream boundary condition) as well as in the last 10 integral scales of the domain are disregarded. This is done to exclude effects of nonstationarity in the velocity field caused by the fixed-head boundary conditions.

[43] Figures 5e and 5f show the probability density functions of concentration along the two length profiles as obtained by the Monte Carlo simulations. The empirical pdfs resemble the analytical results of Figures 5a–5d rather closely. It may be worth noting that the empirical pdfs are based on 50 equally spaced classes of concentration values, whereas the discretization of the concentration space is much finer in the analytical results, particularly close to the extreme values. Thus, the analytical plots in Figures 5a–5d are deliberately constructed with the intention of highlighting high probability density value at the extremes, whereas the latter was not possible using only 10,000 realizations in the Monte Carlo simulations.

[44] In order to quantify the agreement between the numerical and analytical concentration pdfs, we compute the mean absolute difference between the simulated and theoretical distributions in analogy to equation (22). Figure 7 shows the respective length profiles. The comparison between the numerical results and the theoretical concentration pdfs neglecting the variability of transverse mixing is shown as gray lines, whereas the comparison to the theoretical concentration pdfs considering the variability of transverse mixing

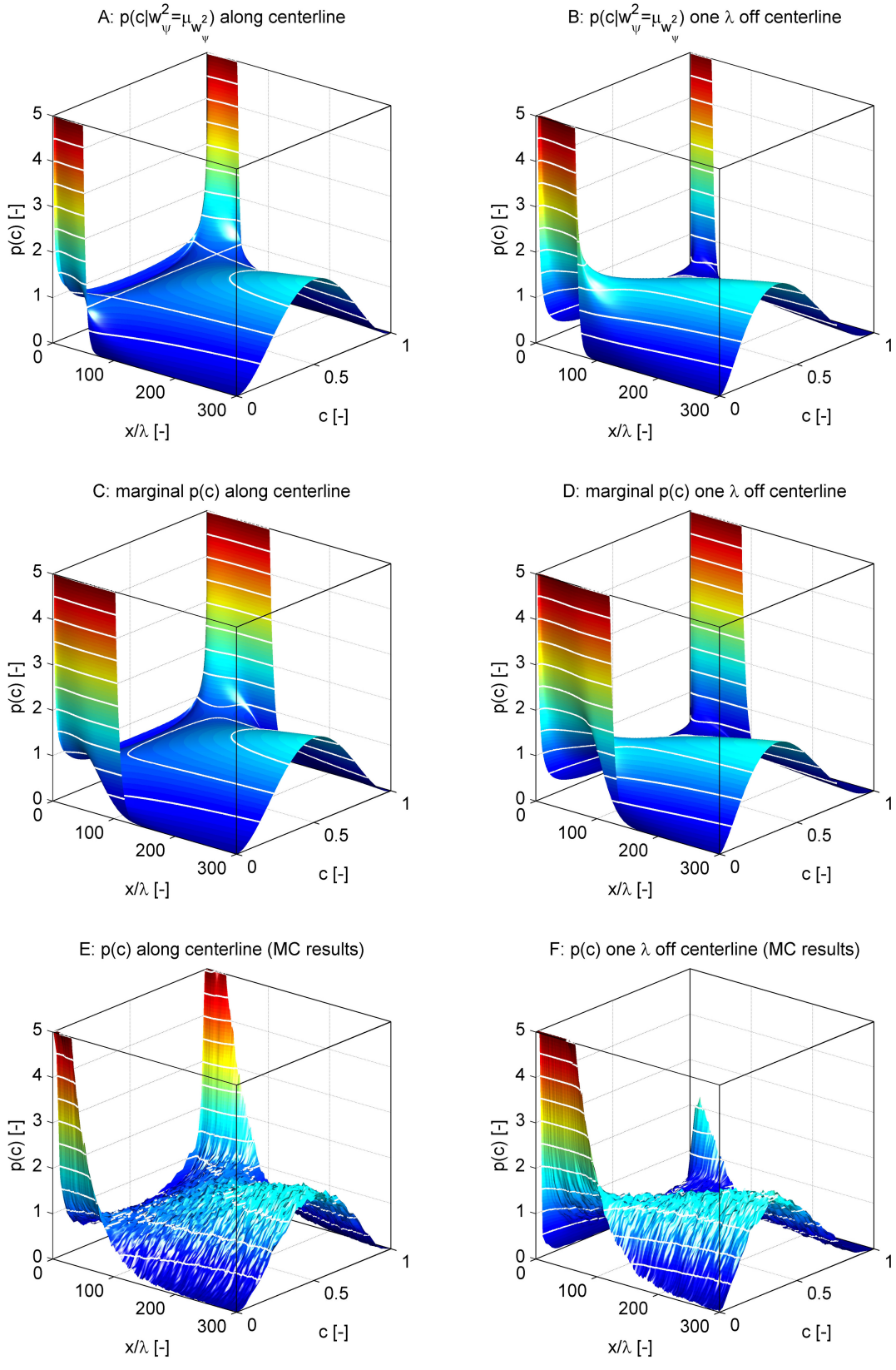
A: p(c|w²ψ=μw²ψ) along centerline
B: p(c|w²ψ=μw²ψ) one λ off centerline
C: marginal p(c) along centerline
D: marginal p(c) one λ off centerline
E: p(c) along centerline (MC results)
F: p(c) one λ off centerline (MC results)
p(c) [-]
x/λ [-]
c [-]
0
100
200
300
0.5
1
2
3
4
5

Figure 5

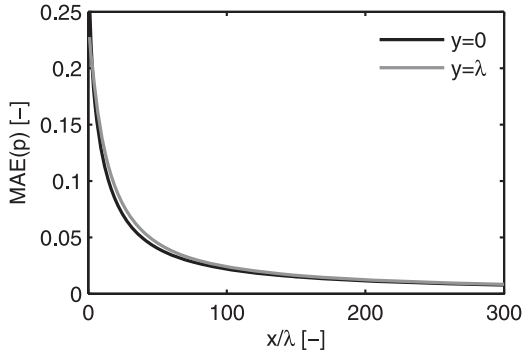

Figure 6. Mean absolute error in probability density introduced by neglecting the uncertainty of w^2_ψ as function of distance. Profile along the centerline of the plume fringe (black line); profile offset by one correlation length (gray line).

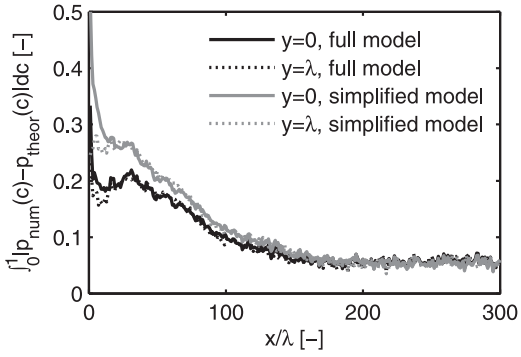

Figure 7. Mean absolute difference in probability density of concentration between the results of numerical Monte Carlo simulations and stochastic-analytical results. Theoretical model including the uncertainty of transverse mixing (black lines), equation (21); theoretical model neglecting the uncertainty of transverse mixing (gray lines), equation (19); length profiles along the centerline of the plume fringe (solid lines); length profiles with one correlation length offset to the centerline (dotted lines).

is shown as black lines. The centerline profiles are solid lines, and the profiles parallel to it are shown as dotted lines.

[45] At very short travel distances, the difference between numerical and analytical results is particularly pronounced. This may be explained with the underlying assumption of the stream function values ψ being normally distributed. In Appendix C, we analyze that the longitudinal distance between two points should be about 10–15 integral scales for the stream function difference to become approximately normally distributed. At very large travel distances, one would expect that the mean absolute difference between theoretical and numerical probability density approaches 0. However, in the given numerical setup, the lateral no-flow boundaries affect the concentration distribution in the interior at sufficiently large travel distances.

[46] Figure 7 shows that both theoretical models of the concentration pdf are in acceptable agreement with the numerical simulations. Note that, by construction, the mean value of probability density $p(c)$ is unity. The theoretical marginal distribution $p(c)$ accounting for the uncertainty of w^2_ψ always performs better than the theoretical conditional distribution $p(c|w^2_\psi = \mu_{w^2_\psi})$, in which w^2_ψ is fixed to its expected value. The difference in the performance of $p(c)$ and $p(c|w^2_\psi = \mu_{w^2_\psi})$ is very much in agreement with the results shown in Figure 6. From this it follows that accounting for the variability of transverse mixing is more important in the regime where the concentration pdf is bimodal, that is, with our parameter set at travel distances of a few tens of integral scales, than in the regime where the pdf turns to be unimodal, i.e., at distances beyond 60 integral scales in our setup.

4. Summary and Conclusions

[47] We have derived analytical expressions for the probability density function of steady state concentration in two-dimensional heterogeneous media with a Heaviside boundary condition, resembling the fringe of an extended plume. Our results are valid on the Darcy scale, i.e., on the smallest possible scale where porous media may be represented as continua, and we parametrize pore scale local dispersion by the Scheidegger parameterization. Our resulting expressions explicitly account for uncertain transverse mixing across streamlines and uncertain position of streamlines. The former causes an uncertain width of the fringe, while the latter causes meandering, squeezing, and stretching of the plume fringe. For the case in which uncertainty of transverse mixing is neglected, we could derive a fully analytical expression, whereas the expression for the case of uncertain mixing contains an integral that we solve numerically.

[48] In addition to the offset from the centerline of the plume fringe, the concentration pdf at a given point x can be categorized into three characteristic regimes, which are governed by the three quantities plotted in Figure 4 for our specific test case: (1) The variance of the stream function value $\sigma^2_\psi(x)$, quantifying meandering of the plume fringe, (2) the expected value of the squared fringe width $\mu_{w^2_\psi}(x)$ in stream function values, quantifying mean effective transverse mixing, and (3) the standard deviation $\sigma_{w^2_\psi}(x)$ of the latter, quantifying the uncertainty of transverse mixing. All three quantities are affected by hydraulic heterogeneity: the larger the variance of log conductivity σ^2_Y, the higher are all three quantities. This implies that we would not expect general patterns that are dramatically different to our test case if we changed the log conductivity variance. In the low-order expressions used in our study, the integral scale has no effect on $\mu_{w^2_\psi}(x)$, but it does influence $\sigma^2_\psi(x)$ and $\sigma_{w^2_\psi}(x)$. In general, larger integral scales lead to larger uncertainties.

[49] The concentration pdf shows distinct maxima at the extreme values for short distances at which $\sigma^2_\psi(x) > \mu_{w^2_\psi}(x)$.

Figure 5. Probability density function of concentration in the test problem as function of normalized travel distance. (a and b) Analytical results for the conditional distribution $p(c|w^2_\psi = \mu_{w^2_\psi})$ neglecting the uncertainty of w^2_ψ; (c and d) Analytical results for the marginalized distribution $p(c)$ accounting for the uncertainty of w^2_ψ; (e and f) Results obtained by Monte Carlo simulations. (Figures 5a, 5c, 5e) Profile along the centerline of the mean plume fringe ($y = 0$); (Figures 5b, 5d, 5f) Profile along a line parallel to the centerline of the mean plume fringe ($y = \lambda$).

In this regime, the fringe is fairly narrow, and an observation point lies essentially either inside the plume or outside. However, the low probability density of intermediate values depends strongly on the degree of mixing, and the uncertainty $\sigma_{w_\psi^2}$ of the effective squared plume width w_ψ^2 has a significant impact on the exact probability density of intermediate concentrations. For the given parameters tested in our application, this regime prevails for almost 60 integral scales, which may be addressed as a large distance for field-scale investigations. This threshold, however, is significantly affected by the value and the parameterization of the local transverse dispersion coefficient. At distances even larger than that, the plume fringe grows so wide that, in most realizations, intermediate concentration values can be observed even though the plume meanders. In this regime, the coefficient of variation of the effective squared plume width w_ψ^2 is so small that the uncertainty $\sigma_{w_\psi^2}$ may be neglected.

[50] Overall the shape of the concentration pdf is dominated by the meandering of streamlines and the mean plume width. The uncertainty of the plume width only leads to minor to moderate modifications of the concentration pdf, even though it quantifies the uncertainty of mixing and dilution. This implies that existing approaches to obtain the concentration pdf that neglect the uncertainty of mixing are not fundamentally biased [*Pannone and Kitanidis*, 1999; *Fiorotto and Caroni*, 2002, 2003; *Caroni and Fiorotto*, 2005; *Schwede et al.*, 2008; *Dentz and Tartakovsky*, 2010]. Yet, they can lead to incomplete statistics of mixing when used as input to mixing-controlled reactive transport scenarios. Our concentration pdf additionally accounts for the uncertainty of mixing, which increases the uncertainty of effective reaction rates under such conditions.

[51] The analytical results derived in this paper require (1) a two-dimensional infinite domain, (2) a lognormal distribution of hydraulic conductivity with a stationary isotropic exponential covariance function of ln(K), (3) mild heterogeneity, and (4) a flow field that is uniform in the mean, free of sources and sinks, and hence statistically stationary. Based on numerical results shown in Appendix C, we assume that (5) stream function values follow a Gaussian distribution, (6) transverse concentration profiles follow an error-function if expressed in stream function values rather than spatial coordinates, and (7) the squared width of these profiles follows a lognormal distribution. We make use of low-order stochastic-analytical results regarding the mean value and uncertainty of cumulative transverse mixing [*Cirpka et al.*, 2011] as well as the uncertainty of stream function differences [*de Barros and Nowak*, 2010].

[52] Our analytical results have successfully been compared to Monte Carlo simulations for a moderate degree of heterogeneity. Several extensions in future work would be desirable. Considering an anisotropic covariance model, maybe of a different functional shape, is mainly a technical question. Extensions to three spatial dimensions, by contrast, are fundamentally different because our derivations depend on the concept of stream functions. In three dimensions, flow lines are subject to vorticity in heterogeneous media, such that switching to flow coordinates becomes far from trivial. Another major complication would be given by a nonstationary log conductivity field, which would be expected when considering distances of tens of integral scales, as done in our study.

Appendix A: Statistics of Stream Function Value ψ (x, y) for Isotropic Exponential Covariance Function of ln(K)

[53] For simplicity, we assume that the hydraulic conductivity field $K(x, y)$ is a multivariate lognormal random spatial variable with isotropic exponential covariance function of its logarithm:

$$K(x,y) = K_g \exp[Y'(x,y)], \tag{A1}$$

$$\langle Y' \rangle = 0, \tag{A2}$$

$$\langle Y'(\xi,\eta) Y'(\xi+\Delta\xi, \eta+\Delta\eta)\rangle = \sigma_y^2 \exp(-\tilde{r}), \tag{A3}$$

in which K_g [L/T] is the geometric mean of K, Y' [-] is the perturbation of log conductivity about its mean, σ_y^2 [-] is the variance of log conductivity, ξ, η [-] denote spatial coordinates normalized by the correlation length λ [L], and $\tilde{r}$ [-] is the normalized distance between two points:

$$\xi = \frac{x}{\lambda}; \eta = \frac{y}{\lambda}; \tilde{r} = \sqrt{\Delta\xi^2 + \Delta\eta^2}. \tag{A4}$$

[54] For the variance of ψ, we extend the derivation of *de Barros and Nowak* [2010], which is based on the analogy of head statistics with stream function statistics, to arbitrary normalized coordinates (ξ, η):

$$\sigma_\psi^2(\xi,\eta) = 2K_g^2 \gamma_\varphi(\xi,\eta), \tag{A5}$$

with

$$\gamma_\varphi(\xi,\eta) = J^2\sigma_Y^2\lambda^2\left\{\Gamma_2(\tilde{r}) + \left(\frac{\eta}{\tilde{r}}\right)^2[\Gamma_1(\tilde{r}) - \Gamma_2(\tilde{r})]\right\}, \tag{A6}$$

$$\Gamma_1(\tilde{r}) = \frac{1}{2}\left[\frac{1}{2} + \frac{\exp(-\tilde{r})(\tilde{r}^2+3\tilde{r}+3)-3}{\tilde{r}^2} + E_1(\tilde{r}) + \ln(\tilde{r}) + \exp(-\tilde{r}) - 0.4228\right], \tag{A7}$$

$$\Gamma_2(\tilde{r}) = \Gamma_1(\tilde{r}) - \left[\frac{1}{2} + \frac{\exp(-\tilde{r})(\tilde{r}^2+3\tilde{r}+3)-3}{\tilde{r}^2}\right], \tag{A8}$$

in which $E_1(\xi) = \int_\xi^\infty \exp(-t)/t\,dt$ is the exponential integral function.

Appendix B: Statistics of Squared Fringe Width for Linear Model of Local Transverse Dispersion

[55] Here, we repeat the low-order perturbative results of *Cirpka et al.* [2011] on the squared fringe width w_ψ^2 in stream function values. The underlying model of local-scale transverse dispersion is the common linear parameterization of *Scheidegger* [1961]:

$$D_t = D_p + \frac{\alpha_t}{\theta} q, \tag{B1}$$

with the pore diffusion coefficient D_p [L^2/T] and the local transverse dispersivity α_t [L] assumed uniform. Assuming an isotropic exponential covariance function of log-hydraulic conductivity, *Cirpka et al.* [2011] derived the following low-order analytical results for the expected value of w_ψ^2:

$$\mu_{w_\psi^2}(x) \approx 2\left[\left(1+\frac{1}{2}\sigma_Y^2\right)D_p\theta K_g J + \left(1+\sigma_Y^2+0.7\sigma_Y^4\right)\alpha_t K_g^2 J^2\right]x, \tag{B2}$$

and its coefficient of variation:

$$CV_{w_\psi^2}(\xi) \approx \frac{\sigma_Y}{\xi\left(D_p + \frac{\alpha_t}{\theta} JK_g\right)} \sqrt{3K_g^2 J^2 \frac{\alpha_t^2}{\theta^2} \mathscr{A}_1(\xi) + 4\left(D_p + \frac{\alpha_t}{\theta} JK_g\right) \frac{\alpha_t}{\theta} JK_g \mathscr{A}_2(\xi) + 2\left(D_p + \frac{\alpha_t}{\theta} JK_g\right)^2 \mathscr{A}_3(\xi)} \tag{B3}$$

with

$$\mathscr{A}_1(\xi) \equiv -E_1(\xi) + \frac{\exp(-\xi)}{\xi^2} - \frac{1}{\xi^2} + \frac{2}{3}\xi + \frac{\exp(-\xi)}{\xi} - \ln(\xi) - \gamma + \frac{1}{2}, \tag{B4}$$

$$\mathscr{A}_2(x) \equiv \xi - E_1(\xi) - \gamma - \ln(\xi), \tag{B5}$$

$$\mathscr{A}_3(x) \equiv \exp(-\xi) - 1 + \xi, \tag{B6}$$

in which $\gamma \approx 0.577216$ is the Euler-Mascheroni constant.

Appendix C: Tests on Assumed Underlying Statistical Distributions

[56] Our derivation of the concentration pdf relies on assumptions about several distributions, namely: (1) the statistical distribution of the difference ψ in the stream function between any point within the domain and the plume fringe at the inflow boundary, equation (11); (2) the statistical distribution of the squared effective width w_ψ^2 of the plume fringe in stream function coordinates, equation (15); and (3) the shape of the spatial concentration distribution $c(\psi)$ in stream function coordinates, equation (7). In order to test these assumptions, we use the Monte Carlo simulations of flow and transport discussed in section 3.2.

[57] As metric for the agreement between the empirical cumulative distribution P_{num} of our numerical Monte Carlo simulations and a theoretical cumulative distribution function P_{theor}, we use the Cramér-von-Mises criterion ω:

$$\omega = \sqrt{\int_0^1 [P_{\text{num}}(v) - P_{\text{theor}}(v)]^2 dP_{\text{theor}}(v)}, \tag{C1}$$

in which v is the variable of interest. Note that in standard normality testing, ω^2 is used rather than ω.

[58] The first test is on the statistical distribution of ψ according to equation (11). We analyze the scaled statistical distribution of ψ along two profiles oriented in the direction of the mean velocity. The first profile follows the mean centerline of the plume fringe, whereas the second profile follows in parallel at a distance of one integral scale. Scaling is done by subtracting the mean and subsequent division by the standard deviation of $\psi(x)$ at each location of interest.

[59] Figure C1a shows the histogram of the scaled ψ-values at the point $x = 103\lambda; y = \lambda$ as an example. Quite obviously, this distribution resembles a standard normal distribution. The corresponding ω-value is 3.9×10^{-8}. Figure C1b shows the value of the Cramér-von-Mises criterion ω along the two profiles as function of distance. Starting at values > 0.02 for small distances, ω drops to values between 0.001 and 0.003 at distances of 10 to 15 integral scales. According to *Anderson and Darling* [1952], the critical value of ω for a significance level of 5% is 1.9×10^{-8} for a sample with 10^4 members. That is, the large number of realizations used in this study shows that ψ is not exactly Gaussian distributed at all points. However, Figure C1a illustrates that the Gaussian distribution is a very good approximation of $p(\psi)$ for $x \gtrapprox 10\lambda$ for the purpose of our study.

[60] The second test is on the statistical distribution of the squared effective width w_ψ^2, which we assume to be lognormal in equation (15). Figure C2a shows a histogram of the scaled $\ln(w_\psi^2)$-values for a distance of $x = 50\lambda$, which should follow a Gaussian distribution after applying the logarithm. At this distance, ω equals 5.3×10^{-8}. As shown in Figure C2b, where ω is plotted as function of distance, ω approaches a value in the order of 0.005 at distances of $x \gtrapprox 15\lambda$. For a sample containing 10^4 realizations, this value leads to a formal failure of the normality test. However, because the inspected distributions strongly resemble Gaussian ones, we assess this sufficient to declare the lognormal distribution to be a good approximation of $p(w_\psi^2)$ for the purposes of you study.

[61] The third test is on the concentration distribution in stream function coordinates according to equation (7).

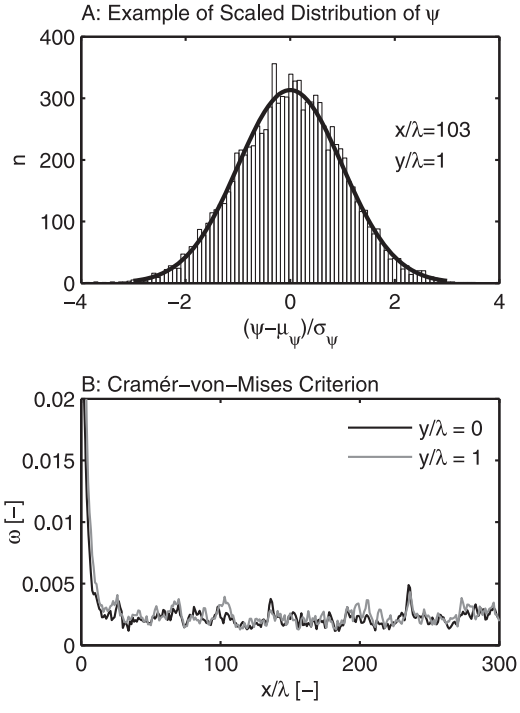

Figure C1. Comparison between the statistical distribution of the normalized difference in stream function values with a standard normal distribution. (top) Histogram of ψ at the location $x/\lambda = 103, y/\lambda = 1$. (bottom) Cramér-von-Mises criterion ω according to equation (C1) for $P[\psi(\mathbf{x})]$ as a function of distance. ω-values for $y = 0$ (black line); ω-values for $y = \lambda$ (gray line). Parameters of the calculations are listed in Table 1.

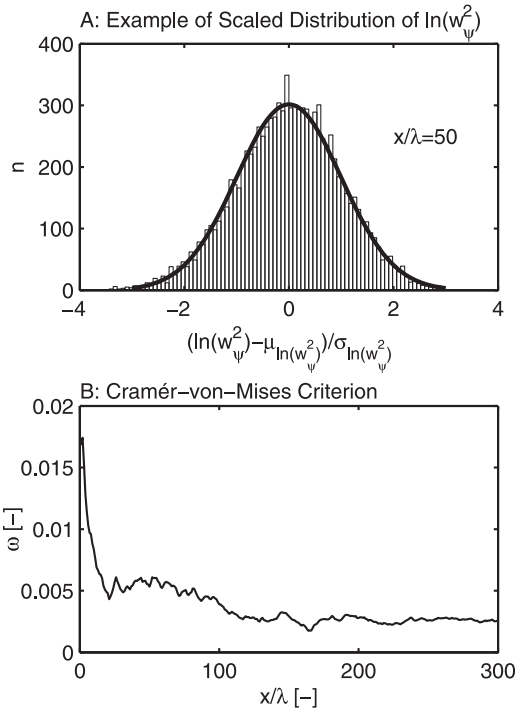

Figure C2. Comparison between the statistical distribution of the normalized logarithmic squared fringe width $\ln(w_\psi^2)$ with a standard normal distribution. (top) Histogram of $\ln(w_\psi^2)$ at the distance $x/\lambda = 50$. (bottom) Cramér-von-Mises criterion ω for $P(w_\psi^2)$ according to equation (C1) as a function of distance. Parameters of the calculations are listed in Table 1.

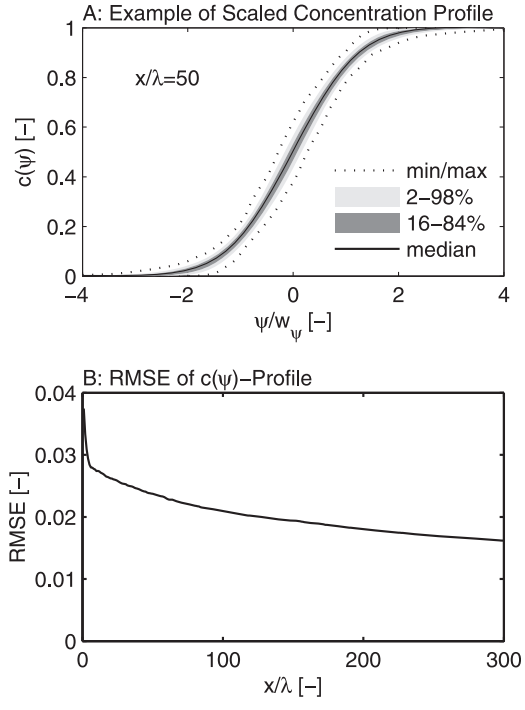

Figure C3. Comparison between scaled transverse concentration distribution and profile according to equation (7). (top) Quantiles of scaled transverse concentration profiles at the distance $x/\lambda = 50$. (bottom) Root-mean-square error according to equation (C2) as a function of distance. Parameters of the calculations are listed in Table 1.

Here, we take the 10,000 realizations of concentration discussed in section 3.2 and compare the numerical concentration profiles $c(\psi)$ for various distances x with the error-function approximation of equation (7). As goodness of fit, we consider the root-mean-square error in the transverse concentration profiles:

$$\mathrm{RMSE}[c(x)] = \sqrt{\left\langle \int_0^1 [c_{\mathrm{num}}(x,\psi) - c_{\mathrm{theor}}(x,\psi)]^2 \, dc_{\mathrm{theor}}(x,\psi) \right\rangle}, \tag{C2}$$

in which $\langle\cdot\rangle$ is the average over the ensemble. The theoretical concentration distribution $c_{\mathrm{theor}}(x,\psi)$ is the error-function profile according to equation (7) with the same center location and width w_ψ as the numerical profile. By integrating over $c_{\mathrm{theor}}(x,\psi)$ rather than ψ, we obtain a dimensionless quantity that is equivalent to the Cramér-von-Mises criterion ω used to express the appropriateness of (log)-normal distributions for $\psi(x)$ and w_ψ^2.

[62] Figure C3a shows the example of a transverse concentration profile $c(\psi)$ for the distance $x = 50\lambda$. The transverse coordinate ψ in each realization is normalized by the individual fringe width w_ψ. Figure C3a shows the corresponding quantiles of $c(\psi/w_\psi)$ over the ensemble of 10,000 realizations. Quite obviously, the distribution resembles the assumed error-function profile of equation (7). Figure C3b shows the corresponding error measure RMSE[$c(x)$] as function of distance. A rapid decrease within the first five integral scales leads to RMSE-values < 0.003, followed by a gradual decrease. We again assess that, for the purpose of our study, the approximation of $c(\psi)$ by equation (7) is sufficient, even though the profiles do not exactly follow the assumed shape.

[63] **Acknowledgments.** This study was supported by the Deutsche Forschungsgemeinschaft (DFG) via the Research Unit 525 "Analysis and modeling of diffusion/dispersion-limited reactions in porous media" (grants GR 971/18-1,18-3) at the University of Tübingen and via the Cluster of Excellence in Simulation Technology (EXC 310/1) at the University of Stuttgart. The second author acknowledges the support of the Spanish Ministry of Science via the "Juan de la Cierva" program. We thank three anonymous reviewers and Alberto Guadagnini for their constructive remarks helping to improve the quality of the paper. The third author acknowledges the support of the EU 7th Framework Programme Collaborative Research Project CLIMB (Climate Induced Changes on the Hydrology of Mediterranean Basins, grant 244151).

References

Anderson, A. W., and D. A. Darling (1952), Asymptotic theory of certain "goodness of fit" criteria based on stochastic processes, *Annals Math. Stat.*, *23*(2), 193–212.

Anneser, B., F. Einsiedl, R. U. Meckenstock, L. Richters, F. Wisotzky, and C. Griebler (2008), High-resolution monitoring of biogeochemical gradients in a tar oil-contaminated aquifer, *Appl. Geochem.*, *23*(6), 1715–1730, doi:10.1016/j.apgeochem.2008.02.003.

Bear, J. (1972), *Dynamics of Fluids in Porous Media*, Elsevier, New York.

Bellin, A., and D. Tonina (2007), Probability density function of non-reactive solute concentration in heterogeneous porous formations, *J. Contam. Hydrol.*, *94*(1–2), 109–125.

Bellin, A., G. Severino, and A. Fiori (2011), On the local concentration probability density function of solutes reacting upon mixing, *Water Resour. Res.*, *47*(1), W01514, doi:10.1029/2010WR009696.

Caroni, E., and V. Fiorotto (2005), Analysis of concentration as sampled in natural aquifers, *Transp. Porous Media*, *59*(1), 19–45.

Chatwin, P., and P. Sullivan (1990), A simple and unifying physical interpretation of scalar fluctuation measurements from many turbulent shear flows, *J. Fluid Mech. 212*, 533–556.

Chiogna, G., O. A. Cirpka, P. Grathwohl, and M. Rolle (2011), Transverse mixing of conservative and reactive tracers in porous media: Quantification through the concepts of flux-related and critical dilution indices, *Water Resour. Res.*, *47*(2), W02505, doi:10.1029/2010WR009608.

Cirpka, O. A. (2010), Simplified simulation of steady state bioreactive transport with kinetic solute uptake by the biomass, *Water Resour. Res.*, *46*(7), W07534, doi:10.1029/2009WR008977.

Cirpka, O., and P. Kitanidis (2000), Characterization of mixing and dilution in heterogeneous aquifers by means of local temporal moments, *Water Resour. Res.*, *36*(5), 1221–1236, doi:10.1029/1999WR900354.

Cirpka, O. A., and A. J. Valocchi (2007), Two-dimensional concentration distribution for mixing-controlled bioreactive transport in steady state, *Adv. Water Resour. 30*(6–7), 1668–1679, doi:10.1016/j.advwatres.2006.05.022.

Cirpka, O. A., and A. J. Valocchi (2009), Reply to comments on "Two-dimensional concentration distribution for mixing-controlled bioreactive transport in steady state" by H. Shao et al., *Adv. Water Resour.*, *32*(2), 298–301, doi:10.1016/j.advwatres.2008.10.018.

Cirpka, O. A., E. O. Frind, and R. Helmig (1999a), Streamline-oriented grid-generation for transport modelling in two-dimensional domains including wells, *Adv. Water Resour.*, *22*(7), 697–710.

Cirpka, O. A., E. O. Frind, and R. Helmig (1999b), Numerical methods for reactive transport on rectangular and streamline-oriented grids, *Adv. Water Resour.*, *22*(7), 711–728.

Cirpka, O. A., Å. Olsson, Q. Ju, M. A. Rahman, and P. Grathwohl (2006), Determination of transverse dispersion coefficients from reactive plume lengths, *Ground Water*, *44*(2), 212–221, doi:10.1111/j.1745-6584.2005.00124.x.

Cirpka, O. A., R. L. Schwede, J. Luo, and M. Dentz (2008), Concentration statistics for mixing-controlled reactive transport in random heterogeneous media, *J. Contam. Hydrol.*, *98*(1–2), 61–74, doi:10.1016/j.jconhyd.2008.03.005.

Cirpka, O. A., F. P. J. de Barros, G. Chiogna, M. Rolle, and W. Nowak (2011), Stochastic flux-related analysis of transverse mixing in two-dimensional heterogeneous porous media, *Water Resour. Res.*, *47*(6), W06515, doi:10.1029/2010WR010279.

Dagan, G. (1984), Solute transport in heterogeneous porous formations, *J. Fluid Mech.*, *145*, 151–177.

Dagan, G. (1985), Stochastic modeling of groundwater flow by unconditional and conditional probabilities: The inverse problem, *Water Resour. Res.*, *21*(1), 65–72, doi:10.1029/WR021i001p00065.

Dagan, G. (1987), Theory of solute transport by groundwater, *Ann. Rev. Fluid Mech.*, *19*(1), 183–213.

Dagan, G. (1989), *Flow and Transport in Porous Formations*, Springer, New York.

de Barros, F. P. J., and W. Nowak (2010), On the link between contaminant source release conditions and plume prediction uncertainty, *J. Contam. Hydrol.*, *116*(1–4), 24–34, doi:10.1016/j.jconhyd.2010.05.004.

de Barros, F. P. J., and Y. Rubin (2011), Modelling of block-scale macrodispersion as a random function, *J. Fluid Mech.*, *676*, 514–545, doi:10.1017/jfm.2011.65.

Dentz, M., and D. M. Tartakovsky (2010), Probability density functions for passive scalars dispersed in random velocity fields, *Geophys. Res. Lett.*, *37*, L24406, doi:10.1029/2010GL045748.

Dentz, M., H. Kinzelbach, S. Attinger, and W. Kinzelbach (2000), Temporal behavior of a solute cloud in a heterogeneous porous medium 1. Point-like injection, *Water Resour. Res.*, *36*(12), 3591–3604, doi:10.1029/2000WR900162.

Dietrich, C. R., and G. N. Newsam (1993), A fast and exact method for multidimensional Gaussian stochastic simulations, *Water Resour. Res.*, *29*(8), 2861–2869, doi:10.1029/93WR01070.

Fiori, A., and G. Dagan (2000), Concentration fluctuations in aquifer transport: A rigorous first-order solution and applications, *J. Contam. Hydrol.*, *45*(1–2), 139–163.

Fiorotto, V., and E. Caroni (2002), Solute concentration statistics in heterogeneous aquifers for finite Peclet values, *Transp. Porous Media*, *48*(3), 331–351.

Fiorotto, V., and E. Caroni (2003), Solute concentration statistics in heterogeneous aquifers for finite Peclet values: Correction, *Transp. Porous Media*, *50*(3), 373.

Frind, E. O., and G. B. Matanga (1985), The dual formulation of flow for contaminant transport modeling: 1. Review of theory and accuracy aspects, *Water Resour. Res.*, *21*(2), 159–169, doi:10.1029/WR021i002p00159.

Gelhar, L. W. (1993), *Stochastic Subsurface Hydrology*, Prentice-Hall, Englewood Cliffs, N.J.

Gelhar, L. W., and C. L. Axness (1983), Three-dimensional stochastic analysis of macrodispersion in aquifers, *Water Resour. Res.*, *19*(1), 161–180, doi:10.1029/WR019i001p00161.

Girimaji, S. S. (1991), Assumed beta-pdf model for turbulent mixing: Validation and extension to multiple scalar mixing, *Combust. Sci. Technol.*, *78*(4–6), 177–196.

Ham, P. A. S., R. J. Schotting, H. Prommer, and G. B. Davis (2004), Effects of hydrodynamic dispersion on plume lengths for instantaneous bimolecular reactions, *Adv. Water Resour.*, *27*(8), 803–813, doi:10.1016/j.advwatres.2004.05.008.

Kapoor, V., and L. W. Gelhar (1994a), Transport in three-dimensionally heterogeneous aquifers: 1. Dynamics of concentration fluctuations, *Water Resour. Res.*, *30*(6), 1775–1788, doi:10.1029/94WR00076.

Kapoor, V., and L. W. Gelhar (1994b), Transport in three-dimensionally heterogeneous aquifers. 2. Predictions and observations of concentration fluctuations, *Water Resour. Res.*, *30*(6), 1789–1801, doi:10.1029/94WR00075.

King, M. W. G., and J. F. Barker (1999), Migration and natural fate of a coal tar creosote plume 1. Overview and plume development, *J. Contam. Hydrol.*, *39*(3–4), 249–279, doi:10.1016/S0169-7722(99)00039-X.

Lichtner, P. C., and D. M. Tartakovsky (2003), Stochastic analysis of effective rate constant for heterogeneous reactions, *Stochastic Environ. Res. Risk Assess.*, *17*(6), 419–429.

Liedl, R., A. J. Valocchi, P. Dietrich, and P. Grathwohl (2005), Finiteness of steady state plumes, *Water Resour. Res.*, *31*(12), W12501, doi:10.1029/2005WR004000.

Lonborg, M. J., P. Engesgaard, P. L. Bjerg, and D. Rosbjerg (2006), A steady state redox zone approach for modeling the transport and degradation of xenobiotic organic compounds from a landfill site, *J. Cont. Hydrol.*, *87*(3–4), 191–210.

Maier, U., and P. Grathwohl (2006), Numerical experiments and field results on the size of steady state plumes, *J. Contam. Hydrol.*, *85*(1–2), 33–52, doi:10.1016/j.jconhyd.2005.12.012.

Meyer, D. W., P. Jenny, and H. A. Tchelepi (2010), A joint velocity-concentration pdf method for tracer flow in heterogeneous porous media, *Water Resour. Res.*, *46*(12), W12522, doi:10.1029/2010WR009450.

Neuman, S. P., C. L. Winter, and C. M. Newman (1987), Stochastic theory of field-scale Fickian dispersion in anisotropic porous media, *Water Resour. Res.*, *23*(3), 453–466, doi:10.1029/WR023i003p00453.

Nowak, W., and O. A. Cirpka (2006), Geostatistical inference of conductivity and dispersion coefficients from hydraulic heads and tracer data, *Water Resour. Res.*, *42*, W08416, doi:10.1029/2005WR004832.

Pannone, M., and P. K. Kitanidis (1999), Large-time behavior of concentration variance and dilution in heterogeneous formations, *Water Resour. Res.*, *35*(9), 623–634, doi:10.1029/1998WR900063.

Peter, A., A. Steinbach, R. Liedl, T. Ptak, W. Michaelis, and G. Teutsch (2004), Assessing microbial degradation of o-xylene at field-scale from the reduction in mass flow rate combined with compound-specific isotope analyses, *J. Contam. Hydrol.*, *71*(1–4), 127–154, doi:10.1016/j.jconhyd.2003.09.006.

Pope, S. (1994), Lagrangian PDF methods for turbulent flows, *Ann. Rev. Fluid Mech.*, *26*(1), 23–63.

Pope, S. B. (1985), Pdf methods for turbulent reactive flows, *Prog. Energy Combust. Sci.*, *11*(2), 119–192.

Prommer, H., N. Tuxen, and P. L. Bjerg (2006), Fringe-controlled natural attenuation of phenoxy acids in a landfill plume: Integration of field-scale processes by reactive transport modeling, *Environ. Sci. Technol.*, *40*(15), 4732–4738, doi:10.1021/es0603002.

Rahman, M. A., S. C. Jose, W. Nowak, and O. A. Cirpka (2005), Experiments on vertical transverse mixing in a large-scale heterogeneous model aquifer, *J. Contam. Hydrol.*, *80*(3–4), 130–148.

Rolle, M., C. Eberhardt, G. Chiogna, O. A. Cirpka, and P. Grathwohl (2009), Enhancement of dilution and transverse reactive mixing in porous media: Experiments and model-based interpretation, *J. Contam. Hydrol.*, *110*(3–4), 130–142, doi:10.1016/j.jconhyd.2009.10.003.

Rubin, Y. (2003), *Applied Stochastic Hydrogeology*, Oxford Univ. Press, Oxford, U. K.

Rubin, Y., M. Cushey, and A. Bellin (1994), Modeling of transport in groundwater for environmental risk assessment, *Stochastic Hydrol. and Hydraul.*, *8*(1), 57–77.

Sanchez-Vila, X., A. Guadagnini, and D. Fernandez-Garcia (2009), Conditional probability density functions of concentrations for mixing-controlled reactive transport in heterogeneous aquifers, *Math. Geosci.*, *41*(3), 323–351.

Scheidegger, A. E. (1961), General theory of dispersion in porous media, *J. Geophys. Res.*, *66*(10), 3273–3278.

Schwede, R. L., O. A. Cirpka, W. Nowak, and I. Neuweiler (2008), Impact of sampling volume on the probability density function of steady-state concentration, *Water Resour. Res.*, *44*, W12433, doi:10.1029/2007WR006668.

Tartakovsky, D. M., and S. Broyda (2011), PDF equations for advective-reactive transport in heterogeneous porous media with uncertain properties, *J. Contam. Hydrol.*, *120–121* (Spec. Issue SI), 129–140, doi:10.1016/j.jconhyd.2010.08.009.

Tartakovsky, D., M. Dentz, and P. Lichtner (2009), Probability density functions for advective-reactive transport with uncertain reaction rates, *Water Resour. Res.*, *45*(7), W07414, doi:10.1029/2008WR007383.

Thornton, S. F., S. Quigley, M. J. Spence, S. A. Banwart, S. Bottrell, and D. N. Lerner (2001), Processes controlling the distribution and natural attenuation of dissolved phenolic compounds in a deep sandstone aquifer, *J. Contam. Hydrol.*, *53*(3–4), 233–267, doi:10.1016/S0169-7722(01)00167-X.

Tonina, D., and A. Bellin (2008), Effects of pore-scale dispersion, degree of heterogeneity, sampling size, and source volume on the concentration moments of conservative solutes in heterogeneous formations, *Adv. Water Resour.*, *31*(2), 339–354, doi:10.1016/j.advwatres.2007.08.009.

Vanderborght, J. (2001), Concentration variance and spatial covariance in second-order stationary heterogeneous conductivity fields, *Water Resour. Res.*, *37*(7), 1893–1912, doi:10.1029/2001WR900009.

Werth, C. J., O. A. Cirpka, and P. Grathwohl (2006), Enhanced mixing and reaction through flow focusing in heterogeneous porous media, *Water Resour. Res.*, *42*, W12414, doi:10.1029/2005WR004511.

Yotsukura, N., and W. W. Sayre (1976), Transverse mixing in natural channels, *Water Resour. Res.*, *12*(4), 695–704, doi:10.1029/WR012i004p00695.

Zhang, D. (2002), *Stochastic Methods for Flow in Porous Media*, Academic, San Diego, Calif.

G. Chiogna, Dipartimento di Ingegneria Civile ed Ambientale, University of Trento, via Mesiano 77, 38123 Trento, Italy. (gabriele.chiogna@ing.unitn.it)

O. A. Cirpka, Center for Applied Geoscience, University of Tübingen, Hölderlinstrasse 12, 72074 Tübingen, Germany. (olaf.cirpka@uni-tuebingen.de)

F. P. J. de Barros, Department of Geotechnical Engineering and Geosciences, Universitat Politecnica de Catalunya-BarcelonaTech, Jordi Girona l-3, 08034 Barcelona, Spain. (felipe.de.barros@upc.edu)

W. Nowak, University of Stuttgart, Institute of Hydraulic Engineering (LH2)/SimTech, Pfaffenwaldring 5a, 70569 Stuttgart, Germany. (wolfgang.nowak@iws.uni-stuttgart.de)